ARTICLE

Photodissociation Dynamics of OCS at 207 nm: S(^{1}D$_2$)+CO($X^1\Sigma^+$) Product Channel

Xi-lin Bai[a*], Dong-feng Zhao[b], Yang Chen[b]

a. School of Physics and Information Engineering, Shanxi Normal University, Linfen 041004, China
b. Hefei National Laboratory for Physical Sciences at the Microscale, Department of Chemical Physics, and Synergetic Innovation Center of Quantum Information & Quantum Physics, University of Science and Technology of China, Hefei 230026, China

(Dated: Received on August 25, 2019; Accepted on September 11, 2019)

By using the direct current slice velocity map imaging technique, the polarization experiment for S(^{1}D$_2$) product from the ultraviolet photodissociation of carbonyl sulfide at 207 nm was studied. The angular momentum polarization character of the photofragment S(^{1}D$_2$) was detected via two different resonance enhanced multiphoton ionization intermediate states, ^{1}F$_3$ and ^{1}P$_1$, and four different pump-probe laser polarization geometries. The angular distribution of the corresponding CO($X^1\Sigma^+$) coproducts was extracted and analyzed using the molecular-frame polarization and the laboratory-frame anisotropy models. The observed total kinetic energy release spectrum indicates that there are three dissociation channels, corresponding to the low, medium, and high kinetic energy. The sources of the low and medium kinetic energy channels are consistent with those of bimodal translational energy distribution at longer photolysis wavelengths. The high kinetic energy channel is a new dissociation channel arising from the direct dissociation from the single repulsive A(2^1A$'$) state.

Key words: Photodissociation dynamics, Carbonyl sulfide, Velocity map imaging

I. INTRODUCTION

Carbonyl sulfide (OCS) has long been served as a benchmark system of triatomic molecules in understanding the dissociation mechanism, as well as for the multidimensional potential energy surfaces (PESs) [1–3]. The photodissociation of OCS was thought to be a main source of the stratospheric sulfate aerosol, the sudden decrease of OCS concentration in the stratosphere increased the importance of the shorter wavelength photolysis [4]. And the photolysis products of OCS in the stratospheric UV window are also of great significance in the secondary reaction of the atmosphere [5, 6]. Meanwhile, the photolysis products orbital polarization effect of carbonyl sulfide has attracted enormous interest due to its important information of angular momentum [7–11]. In recent years, extensive experimental [12–25] and theoretical [26–29] studies on the photodissociation dynamics of OCS in ultraviolet (UV) region have been reported.

From the first UV absorption band of OCS [28], we can know that the main source of absorption is caused by excitation of the single repulsive A(2^1A$'$) state, and the main structure observed in the cross section comes from the excitation of the triple bound c(2^3A$''$) state. Besides, there is an extremely weak absorption from the excitation of the single repulsive B(1^1A$''$) state. The spin-allowed channel S(^{1}D$_2$)+CO($X^1\Sigma^+$) dominates in the UV absorption band of OCS [12]. The total kinetic energy release spectrum (TKER) of the main channel shows a bimodal distribution at $\lambda \geq 214$ nm, and a new channel appears at 210 nm [23]. The highly excited rotational product CO measured in experimental work is caused by strong bending on the excited state surfaces. And the higher-J rotational distribution of CO becomes more obvious with the increasing of the excitation energy [3]. The quantum yield of the spin-forbidden channel, S(^{3}P$_J$)+CO($X^1\Sigma^+$), derived from the intersystem crossing is very small.

Investigation of the angular momentum polarization [30–33] of the atomic photofragments of photolysis reactions can provide an insightful understanding of the photodissociation dynamics. For example, the $\boldsymbol{\mu}$-**j** correlation parameter $\beta_0^2(02)$ in the photodissociation of OCS can distinguish the symmetry of the excited state. The determined alignment and anisotropy parameters can distinguish the incoherent excitation and coherent excitation. Recently, these polarization parameters of the atomic S(^{1}D$_2$) photofragments can be determined by using the high-resolution slice imaging technology. Using this method, Sofikitis and co-workers observed the resonant behavior in the photodissociation of OCS at a particular excitation wavelength [11].

*Author to whom correspondence should be addressed. E-mail: bxl5630@mail.ustc.edu.cn

In our previous work, we studied the photodissociation dynamics of OCS at 210 [23] and 217 nm [24] using the slice velocity map imaging (VMI) apparatus. In this work, we report a detailed experimental study on S(^{1}D$_2$) orbital polarization from the photodissociation of OCS at 207 nm, extending to the shorter wavelength. By comparison with the previous experimental data measured from other dissociation wavelengths, a new different dissociation channel is experimentally identified. This work focuses on the detailed discussion on the dissociation mechanism based on the observed anisotropy and polarization parameters, as well as the influence of multidimensional PESs on the photolysis process.

II. EXPERIMENTS

The setup of the time-sliced VMI experiment was described in detail in our previous studies [34–37]. In brief, a pulsed supersonic molecular beam of OCS regent with He was expanded into a source chamber and then directed along the central axis of the time-of-flight (TOF). The skimmed molecular beam passed through a 1-mm diameter hole in the repeller plate of the ion optic, then intersected by the photolysis laser beam. Tens of nanoseconds after photolysis laser, the S(^{1}D$_2$) fragments were probed by the (2+1) REMPI scheme via the ^{1}P$_1$ and ^{1}F$_3$ resonant intermediate states. The photolysis-probe laser beams were parallel to the detection plane, and crossed the molecular beam between the repeller (R) and extractor (E) plates. The ionized S$^+$ ions were accelerated by the ion optics and passed through a TOF tube toward the Chevron dual multichannel plate (MCP, ∼40 mm) detector and provided velocity mapping in the focusing electric fields. Mass selectivity was achieved by applying a ∼50 ns gate pulse with high voltage to the front of the MCP's detector. The resulting images on the P47 phosphor screen were recorded by a gated intensified charge-coupled device camera (Imager Intense, LaVision) in conjunction with the ion event counting. Timing of the pulsed molecular beam, the lamps of the photolysis and probe lasers, and the pulsed gating switched on the detector was controlled by two delay pulse generators (DG 535, Stanford Research System).

For two-color experiments, the linearly polarized photolysis laser beam (207 nm) was achieved by the frequency-tripled output of a dye laser (DCM) pumped by a Nd:YAG laser (Spectra Physics, 532 nm), giving only about 0.3 mJ/pulse, for decreasing the background. The polarization of the photolysis laser beam was controlled by a Berek's polarization rotator (Model 5540, New Focus), and monitored by a MgF_2 Rochon prism. The sulfur probe beam with a pulse energy of 0.8 mJ (set at 288.18 and 291.48 nm for the transition to ^{1}F$_3$ and ^{1}P$_1$ intermediate states respectively) was generated by the frequency-doubled output of the other tunable dye laser (Rhodamine 610), which was pumped by the second harmonic of Nd:YAG laser (Spectra Physics, 532 nm). A quartz half-wave plate (Thorlabs, 260−400 nm) was used to control the relative orientation of the probe laser to be perpendicular to the pulsed molecular beam (noted as V) or parallel to the pulsed molecular beam (noted as H). The photolysis and probe laser beams were spatially overlapped and focused on the interaction region using two focal length lens (f_1=250 mm and f_2=200 mm). The photolysis-probe delay for the whole experiments was optimized at around 20 ns. Narrow scanning of the probe laser was utilized for the S(^{1}D$_2$) fragments in order to avoid the Doppler effect.

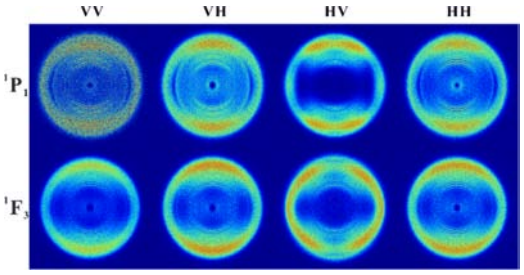

FIG. 1 Raw time-sliced ion images of S(^{1}D$_2$) products from the photodissociation of OCS at 207 nm.

III. OBSERVATIONS AND ANALYSIS

A. Results and analysis

The time-sliced ion images of the S(^{1}D$_2$) photoproducts in FIG. 1 were recorded with the photolysis of OCS at 207 nm. Two different resonant intermediate states of S(^{1}D$_2$) with four different pump-probe laser polarization geometries are employed to obtain the anisotropy and polarization parameters. VH, VV, HH, and HV were used to describe the polarization geometries of the pump-probe laser. For example, the first letter in "VH" geometry represents the polarization of the pump laser and the second letter represents the polarization of the probe laser. Here, the label "V" and "H" indicate the polarization of the laser is perpendicular and parallel to the TOF axis, respectively.

In FIG. 1, each of the sliced images represents a 2D projection of the recoil velocity distribution of the S(^{1}D$_2$) fragments. The clearly separated velocity rings of the S photofragments in the images correspond to the internal energy distribution of the CO($X^1\Sigma^+$) cofragments. According to the law of energy conservation, the total kinetic energy release spectrum in the photodissociation process can be described by the following equation:

$$\mathrm{TKER}=h\nu-D_0(\mathrm{OC-S})-E_{\mathrm{int}}(\mathrm{CO})-E_{\mathrm{int}}(\mathrm{S}) \qquad (1)$$

where $h\nu$ is the photolysis energy of 207 nm, D_0(OC−S)

DOI:10.1063/1674-0068/cjcp1908148

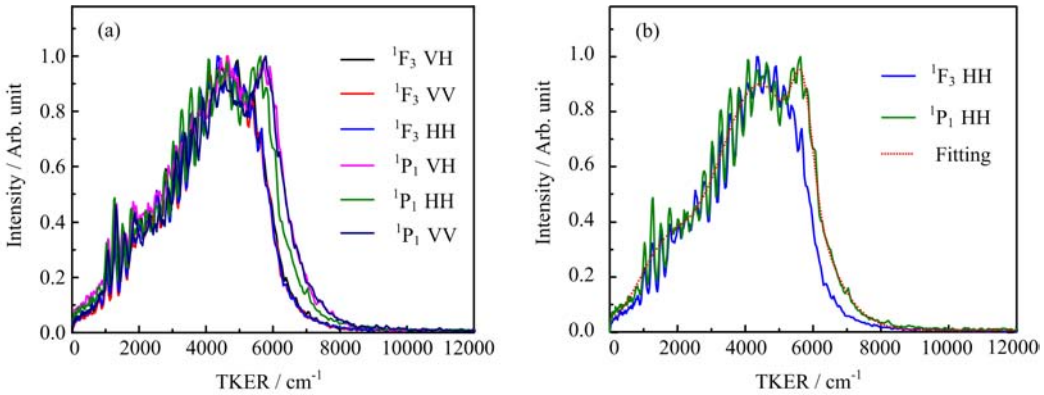

FIG. 2 (a) Total kinetic energy distributions for the S(^{1}D$_2$)+CO($X^1\Sigma^+$) product channel from the photodissociation of OCS at 207 nm. (b) Comparison of TKER spectra in different intermediate states with the same polarization geometry. Fitted curves of the TKER spectra in the HH geometry with the ^{1}P$_1$ as resonant intermediate using three Gaussian functions are illustrated with red dot line.

is the bond energy of the C−S bond that was determined by previous studies, $E_{\rm int}$(CO) and $E_{\rm int}$(S) are the internal energy of the products CO($X^1\Sigma^+$) and S(^{1}D$_2$), respectively. The TKER spectra in the center-of-mass frame were obtained by integrating the time-sliced images overall product velocity angles. FIG. 2 shows the obtained TKER spectra of photodissociation of OCS at 207 nm.

FIG. 2(b) shows that the obtained TKER spectra can be successfully decomposed into three Gaussian components. It means that there are three different dissociation pathways for S(^{1}D$_2$)+CO($X^1\Sigma^+$) channel. The features of low $E_{\rm T}$ component and medium $E_{\rm T}$ component are extremely similar to a bimodal structure for dissociation at longer wavelengths [14, 20], although the two components are almost overlapped and have higher rotational distributions. The high $E_{\rm T}$ component also appears as dissociation at 210 nm which is the opening window for the high $E_{\rm T}$ channel [23]. Besides, the obtained CO rotational distributions exhibit a significant dependence on the REMPI transition of S(^{1}D$_2$). FIG. 2(b) shows that the intensity of the high $E_{\rm T}$ component channel via intermediate state ^{1}P$_1$ is larger than that via intermediate state ^{1}F$_3$. This dependence as interpreted in Ref.[32], indicates the polarized characteristic of photofragment S(^{1}D$_2$). The line strength factors for different REMPI transition schemes may be responsible for this difference.

The angular distributions corresponding to CO($X^1\Sigma^+$), $I(\theta)$, can be extracted from the images by integrating the intensity over the corresponding narrow radial range for each rotational peak and fitted by the following expression:

$$I(\theta)=1+\beta_2 P_2(\cos\theta)+\beta_4 P_4(\cos\theta)+\beta_6 P_6(\cos\theta) \quad (2)$$

where θ is the crossing angle between the recoil velocity of the S(^{1}D$_2$) photofragment and the polarization orientation of the UV photolysis laser, and $P_{k(2,4,6)}$ are the kth-order Legendre polynomials. The Legendre polynomial coefficients $\beta_{k(2,4,6)}$ values were obtained by fitting the angular distributions with Eq.(2) using the least-squares method. The anisotropy parameter and the polarization parameters of S(^{1}D$_2$) from 207 nm photodissociation of OCS can be determined by the Legendre polynomial coefficients $\beta_{k(2,4,6)}$ values using the theoretical model described by Rakitzis and Zare [38].

The angular distributions of S(^{1}D$_2$) from dissociation at 207 nm have J-dependent characteristics. For the HV pump-probe laser polarization geometry, the angular distribution of S(^{1}D$_2$) changes obviously in different CO(J). For the low $E_{\rm T}$ component, the peak of $I(\theta)$ is near 0° and 180°. For the medium $E_{\rm T}$ component, the peak of $I(\theta)$ is near 45° and 30° for detection through the ^{1}P$_1$ and ^{1}F$_3$ intermediated states, respectively. For the high $E_{\rm T}$ component, the peak of $I(\theta)$ is returned to 0° and 180°. Besides, the angular distributions of S(^{1}D$_2$) fragments from the photodissociation of OCS at 210 nm and 207 nm are also different, especially for the high $E_{\rm T}$ component in VH pump-probe laser polarization geometry and resonance intermediate ^{1}F$_3$ state. In FIG. 3, another difference for the high $E_{\rm T}$ component is that the β value increases to a higher value of ∼0.78 and the bipolar momentum parameter $\beta_0^2(02)$ value increases to a positive value with the decreasing of the rotational quantum number of CO. Both of them indicate that there are different dissociation mechanisms in photodissociation at 210 and 207 nm photons.

B. Photoexcitation and photodissociation mechanisms

The A(2^1A′) state plays a critical role in the main dissociation pathways, due to the fact that the main excitation comes from the repulsive A(2^1A′) state through the calculated absorption spectrum [27]. From the previous studies, we can get that the low and medium $E_{\rm T}$ component channels arise from the A(2^1A′) state ex-

DOI:10.1063/1674-0068/cjcp1908148

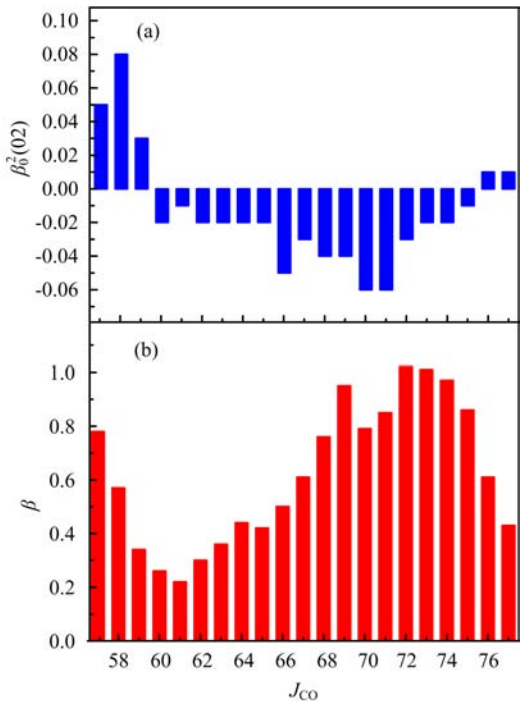

FIG. 3 (a) The bipolar momentum parameters $\beta_0^2(02)$ and (b) the anisotropy parameters β extracted from the time-sliced ion images of $S(^1D_2)$ products produced by dissociation of OCS at 207 nm.

citation followed by the nonadiabatic crossing to the $X(1^1A')$ state and the simultaneous two repulsive states (A and B) excitation, respectively. The extremely high $CO(J)$ rotational distributions for these two components indicate that there is greater bending in the dissociation process. This is in agreement with the previous observations and calculations [21, 28].

The calculated vertical excitation energy of the singlet $A(2^1A')$ state is only 0.06 eV higher than that of the triplet $c(2^3A'')$ state [27]. However, the energy difference between 207 and 210 nm photons is 0.09 eV. Meanwhile, we notice from Ref.[23] that the experimental photoexcitation energy, 210 nm, can reach the vertical excitation region for $c(2^3A'')$ state. Thus, it indicates that our experimental photoexcitation energy ~207 nm can reach the vertical excitation region for $A(2^1A')$ state. The high β parameters observed in the high E_T component just manifest that the symmetry of dissociation excited state is A'. And the low rotational distribution indicates that this channel comes from direct dissociation from the Frank-Condon excitation region. Hence, a direct dissociation from the $A(2^1A')$ state may lead to the generation of the high E_T component channel.

The translational energy distributions are roughly similar to the dissociation results of OCS at 193 nm [17], although the anisotropy parameters of the high E_T component channel become larger. This suggests that the bending degree of molecules by laser excitation is not increased with the increasing of the excitation energy. From the perspective of the PESs, even of the three-atom molecules, the dissociation pathways are also very complex. It needs further theoretical and experimental work accurately to describe molecular dynamics behavior.

For dissociation of triatomic molecule OCS, the transition to an A'' state can obviously result in anisotropic angular distributions with the limiting β value of -1, while the transition to an A' state can generate any value of angular anisotropy, β, between -1 and 2, depending on the intersection angle of the transition dipole moment vector $\boldsymbol{\mu}$ with respect to the recoil vector $\boldsymbol{\nu}$. The strong coupling region between the A state and the ground state is off the transition dipole moment, and the β value of the low E_T component channel can not reach the limiting value of 2. Unfortunately, we did not find the inversion of the recoil direction (recoil resonance) of the high-J CO products [11]. Maybe the excitation position in our experiment is not in the resonance absorption peak position.

An anomalously strong J=81 level presented in the TKER spectra may be induced by a dynamically constrained threshold effect that seems to happen in the photodissociation of HOD [39]. Because there is a centrifugal barrier from the linear ground state to the products via a bending excited state geometry. The inner ring with a negative anisotropy parameter conforms that the photodissociation of hot-band OCS occurs from the repulsive $B(1^1A'')$ state induced by the lonely probe laser.

IV. CONCLUSION

We measured the anisotropy parameter and the polarization parameters of $S(^1D_2)$ arising from the dissociation of OCS+$h\nu$(207 nm)→$S(^1D_2)$+$CO(X^1\Sigma^+)$ using the time-sliced velocity ion imaging technique. The observed total kinetic energy release spectra show that there are three main dissociation channels: the nonadiabatic process between the $A(2^1A')$ state and the ground state for the low E_T component channel, the two-state excitation for the medium E_T component channel, and the direct dissociation from the $A(2^1A')$ state for the high E_T component channel (the new channel). The experiments revealed that the photodissociation mechanism depends on the excitation energy. It is very important to understand the influence of multidimensional PESs from the detailed analysis of the photodissociation mechanism.

V. ACKNOWLEDGMENTS

This work was supported by the National Key R&D Program of China (No.2017YFA0303502), the National Natural Science Foundation of China (No.21773221 and

No.21727804), and the Fundamental Research Funds for the Central Universities of China (No.WK2340000078).

[1] R. Schinke, *Photodissociation Dynamics: Spectroscopy and Fragmentation of Small Polyatomic Molecules*, Cambridge: Cambridge University Press, (1995).
[2] F. F. Crim, J. Phys. Chem. **100**, 12725 (1996).
[3] J. A. Schmidt and J. M. Olsen, J. Chem. Phys. **141**, 184310 (2014).
[4] M. Chin and D. D. Davis, J. Geophys. Res. **100**, 8993 (1995).
[5] J. Notholt, Z. Kuang, C. P. Rinsland, G. C. Toon, M. Rex, N. Jones, T. Albrecht, H. Deckelmann, J. Krieg, C. Weinzierl, H. Bingemer, R. Weller, and O. Schrems, Science **300**, 307 (2003).
[6] P. Ehrenfreund and S. B. Charnley, Annu. Rev. Astron. Astrophys. **38**, 427 (2000).
[7] T. P. Rakitzis, P. C. Samartzis, and T. N. Kitsopoulos, Phys. Rev. Lett. **87**, 123001 (2001).
[8] A. J. Orrewing and R. N. Zare, Annu. Rev. Phys. Chem. **45**, 315 (1994).
[9] T. P. Rakitzis, A. J. van den Brom, and M. H. M. Janssen, Science **303**, 1852 (2004).
[10] A. G. Suits and O. S. Vasyutinskii, Chem. Rev. **108**, 3706 (2008).
[11] D. Sofikitis, J. Suarez, J. A. Schmidt, T. P. Rakitzis, S. C. Farantos, and M. H. M. Janssen, Phys. Rev. Lett. **118**, 253001 (2017).
[12] G. Nan, I. Burak, and P. L. Houston, Chem. Phys. Lett. **209**, 383 (1993).
[13] Y. Sato, Y. Matsumi, M. Kawasaki, K. Tsukiyama, and R. Bersohn, J. Phys. Chem. **99**, 16307 (1995).
[14] Z. H. Kim, A. J. Alexander, and R. N. Zare, J. Phys. Chem. A **103**, 10144 (1999).
[15] A. J. van den Brom, T. P. Rakitzis, and M. H. M. Janssen, J. Chem. Phys. **121**, 11645 (2004).
[16] M. Laura Lipciuc and Maurice H. M. Janssen, Phys. Chem. Chem. Phys. **8**, 3007 (2006).
[17] S. K. Lee, R. Silva, S. Thamanna, O. S. Vasyutinskii, and A. G. Suits, J. Chem. Phys. **125**, 144318 (2006).
[18] M. Brouard, F. Quadrini, and C. Vallance, J. Chem. Phys. **127**, 084305 (2007).
[19] M. L. Lipciuc, T. P. Rakitzis, W. L. Meerts, G. C. Groenenboom, and M. H. Janssen, Phys. Chem. Chem. Phys. **13**, 8549 (2011).
[20] M. P. Grubb, M. L. Warter, C. D. Freeman, N. A. West, K. M. Usakoski, K. M. Johnson, J. A. Bartz, and S. W. North, J. Chem. Phys. **135**, 094201 (2011).
[21] W. Wei, C. J. Wallace, G. C. McBane, and S. W. North, J. Chem. Phys. **145**, 024310 (2016).
[22] C. Weeraratna, C. Amarasinghe, R. Fernando, V. Tiwari, and A. G. Suits, Chem. Phys. Lett. **657**, 162 (2016).
[23] X. Bai, H. Liang, Z. Zhou, Z. Hua, B. Jiang, D. Zhao, and Y. Chen, J. Chem. Phys. **147**, 013930 (2017).
[24] X. Bai, H. Liang, Z. Zhou, Z. Hua, D. Zhao, and Y. Chen, Chin. J. Chem. Phys. **30**, 499 (2017).
[25] D. Sofikitis, J. Suarez, J. A. Schmidt, T. P. Rakitzis, S. C. Farantos, and M. H. M. Janssen, Phys. Rev. A. **98**, 034117 (2018).
[26] S. O. Danielache, S. Nanbu, C. Eskebjerg, M. S. Johnson, and N. Yoshida, J. Chem. Phys. **131**, 24307 (2009).
[27] J. A. Schmidt, M. S. Johnson, G. C. McBane, and R. Schinke, J. Chem. Phys. **136**, 131101 (2012).
[28] G. C. McBane, J. A. Schmidt, M. S. Johnson, and R. Schinke, J. Chem. Phys. **138**, 94314 (2013).
[29] B. W. Toulson and C. Murray, J. Phys. Chem. A **120**, 6745 (2016).
[30] A. S. Bracker, E. R. Wouters, A. G. Suits, Y. T. Lee, and O. S. Vasyutinskii, Phys. Rev. Lett. **80**, 1626 (1998).
[31] A. P. Clark, M. Brouard, F. Quadrinia, and C. Vallancea, Phys. Chem. Chem. Phys. **8**, 5591 (2006).
[32] T. P. Rakitzis and A. J. Alexander, J. Chem. Phys. **132**, 224310 (2010).
[33] C. Weeraratna, O. S. Vasyutinskii, and A. G. Suits, Phys. Rev. Lett. **122**, 083403 (2019).
[34] R. Mao, Q. Zhang, M. Chen, C. He, D. Zhou, X. Bai, L. Zhang, and Y. Chen, J. Chem. Phys. **139**, 166101 (2013).
[35] Z. Gu, M. Chen, C. He, X. Bai, R. Mao, Q. Zhang, and Y. Chen, Chin. J. Chem. Phys. **26**, 493 (2013).
[36] M. Chen, C. He, X. Bai, D. Zhao, and Y. Chen, J. Chem. Phys. **147**, 226101 (2017).
[37] Z. Hua, S. Feng, Z. Zhou, H. Liang, Y. Chen, and D. Zhao, Rev. Sci. Instrum. **90**, 013101 (2019).
[38] T. P. Rakitzis and R. N. Zare, J. Chem. Phys. **110**, 3341 (1999).
[39] S. A. Harich, X. F. Yang, X. Yang, R. Harrevelt, and M. C. Hemert, Phys. Rev. Lett. **87**, 263001 (2001).

DOI:10.1063/1674-0068/cjcp1908148